Fast Switching NO_2-doped p-Channel Diamond MOSFETs

Niloy Chandra Saha, Tomoki Shiratsuchi, Seong-Woo Kim, Koji Koyama, Toshiyuki Oishi, *Senior Member, IEEE*, and Makoto Kasu

***Abstract*— This letter demonstrates the fast-switching characteristics of a normally-on NO_2 p-type doped diamond metal-oxide-semiconductor field-effect transistor (MOSFET). A very fast-switching operation was realized for a diamond MOSFET with a turn-on (t_{on}) and turn-off (t_{off}) time of as low as 9.97 and 9.63 ns, respectively. The parasitic parameters that influence the switching time and switching loss were measured as input capacitance, C_{iss} of 245 nF/mm, output capacitance, C_{oss} of 732 pF/mm, and reverse capacitance, C_{rss} of 17 pF/mm. A total switching energy loss was determined to be only 208 pJ. This report suggests the potential of NO_2-doped diamond MOSFETs for prospective high-speed switching applications.**

***Index Terms*—diamond MOSFET, dynamic characteristics, fast-switching, NO_2 p-type doping**

I. Introduction

DIAMOND is a potential ultrawide bandgap semiconductor material for future high-power and high-frequency transistors. Excellent features of diamond comprise a high bandgap energy of 5.47 eV, high electric breakdown field of >10 MV/cm [1,2], high thermal conductivity of 22 W/cm·K [3], and electron and hole mobilities of 4500 and 3800 $cm^2V^{-1}s^{-1}$, respectively [4]. Impurity doping in diamonds results in a low carrier concentration (ρ_s) owing to their high activation energies (E_A). Hydrogen termination in diamond is an alternative that showed a ρ_s of 10^{12} ~10^{13} cm^{-2} when exposed to air. Hydrogen-terminated diamond (H-diamond) field-effect transistors (FETs) demonstrated exceptional radiofrequency (RF) capabilities with RF power densities of 2.1 and 3.8 W/mm at 1 GHz [5,6], and 4.2 W/mm at 2 GHz [7], maximum cut-off frequency (f_T) and maximum frequency of oscillation (f_{max}) of 70 GHz and 120 GHz, respectively [8,9].

The ρ_s is significantly increased by NO_2 p-type doping in H-diamond up to 2.4×10^{14} cm^{-2}, an order of magnitude higher than that of air [10,11]. An Al_2O_3 layer passivation is required to prevent the desorption of NO_2 molecules and attain thermal stabilization [12]. An NO_2 p-type doped diamond metal–oxide–semiconductor field-effect transistor (MOSFET) was reported with the highest drain current density of 1.35 A/mm [13]. Furthermore, reportedly excellent RF characteristics include 2 W/mm of RF power density at 1 GHz [14]. Recently, high-power operations of NO_2 p-type doped diamond MOSFETs were demonstrated with a maximum Baliga's figure-of-merit of 875 MW/cm^2 [15] and breakdown voltages of >2500 to 3659 V (the highest among diamond MOSFETs) [16-18].

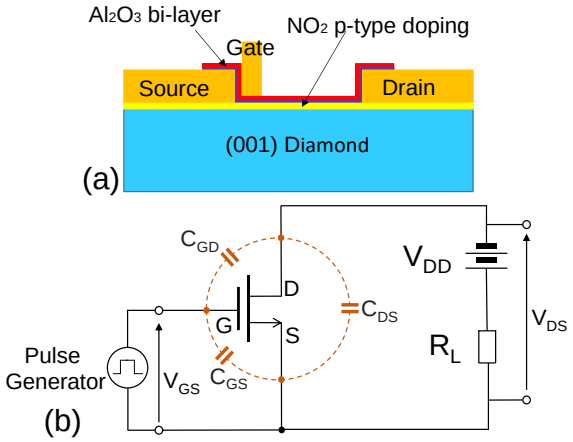

Fig. 1. (a) Schematic cross-section of the Al_2O_3 passivated, NO_2 p-type doped H-diamond MOSFETs. (b) Circuit diagram for the dynamic switching characteristics measurements.

The static characteristics of diamond transistors have been extensively studied [19-24], however the dynamic characteristics are yet to be thoroughly investigated. For power circuit applications, switching characteristics are significant for realizing the switching behavior and the corresponding switching losses. In this study, we present the dynamic switching characteristics of a normally-on NO_2 p-type doped diamond MOSFET. The dynamic characteristics of the MOSFET were realized for the first time, demonstrating a considerably short switching time.

II. Growth and Device Fabrication

Fig. 1(a) shows the schematic cross-section of a NO_2 p-type doped and Al_2O_3 layer passivated diamond MOSFET on misoriented diamond substrates. The misoriented (001) diamond was grown on an Ir buffered $(11\bar{2}0)$, thus A-plane, sapphire substrate misoriented by 3.0° toward the [0001], thus *c*-direction, and the diamond layer was naturally delaminated from the sapphire substrates after the diamond growth during cooling [25].

Manuscript received December 30, 2022. This work was supported by the Japan Society for the Promotion of Science Grants-in-aid for Scientific Research (No. 22H01974).

N. C. Saha, T. Shiratuschi, T. Oishi, and M. Kasu are with the Department of Electrical and Electronic Engineering, Saga University, Saga 840-8502, Japan (e-mail: kasu@cc.saga-u.ac.jp).

S. -W. Kim, and K. Koyama are with Orbray Co., Ltd. Tokyo 123-8511, Japan.

An approximately 100 nm-thick homoepitaxial diamond was grown on the misoriented diamond substrate by exposing it to plasma of H_2 and CH_4 in a microwave plasma chemical vapor deposition system. The ratio of the CH_4/H_2 was 1%. The microwave plasma power was 750 W, and the working pressure was 50 Torr. NO_2 doping was performed by exposing the H-diamond to 2% NO_2 gas diluted in N_2. A 50 nm-thick Au layer was deposited on it, and the source and drain were patterned photolithographically. The active hole channel was again exposed to 2% NO_2 to ensure p-type doping [15].

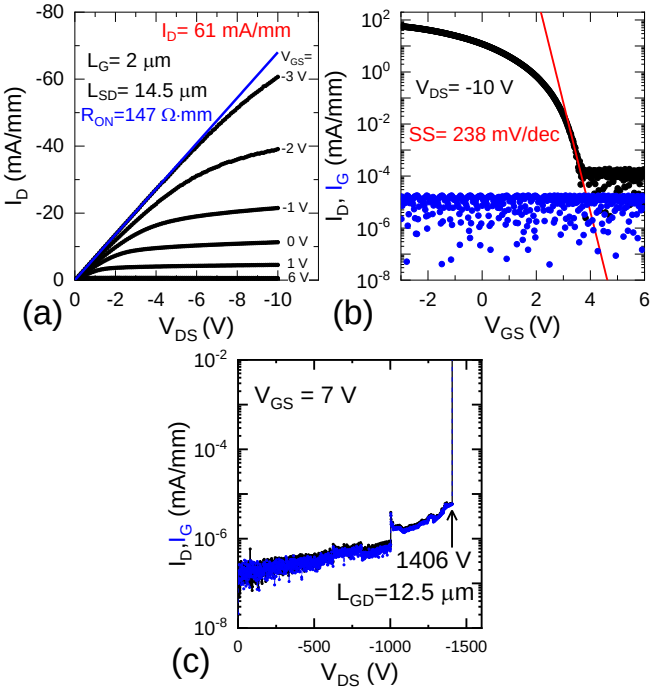

Fig. 2. (a) Drain current-voltage (I_D-V_{DS}) characteristic, (b) I_D, I_G–V_{GS} characteristics, and (c) off-state breakdown voltage characteristics of the diamond MOSFET (L_G= 2 µm, W_G= 45 µm, L_{SD}= 14.5 µm, and L_{GD}=12.5 µm).

Using the atomic layer deposition (ALD) technique, an Al_2O_3 bilayer with a total thickness of 16 nm was deposited as the gate insulating layer and hole channel passivation layer. Trimethylaluminum and H_2O were sequentially supplied as the source gases for Al and O, respectively. The first 4 nm thick Al_2O_3 layer was deposited at 120 °C and the second 12 nm thick Al_2O_3 layer was deposited at 230 °C. A 50 nm-thick Au layer was thermally evaporated onto the Al_2O_3 layer, and the gate was formed adjacent to the source electrode [26]. The gate length (L_G) was 2 µm, and the gate-to-drain length (L_{GD}) and drain-to-source length (L_{SD}) were 12.5, and 14.5, respectively. The MOSFET was bonded to a printed circuit board to prepare a circuit for measuring the dynamic characteristics (Fig. 1(b)). The output characteristics of the MOSFET were measured using a Keysight 1505A power device analyzer, the dynamic switching characteristics were measured using a Rohde & Schwarz RTO 1004 oscilloscope, and a Keysight 81150A wave function generator was used to apply the gate pulse.

III. Results and Discussion

Fig. 2(a) shows the static drain current-voltage (I_D-V_{DS}) output characteristics of the diamond MOSFET. A gate voltage (V_{GS}) was applied from 6 to −3 V in steps of 1 V, while V_{DS} was swept from 0 to −10 V. The MOSFET exhibited an I_D of −61 mA/mm at V_{GS}= −3 V. Maximum transconductance (g_m) was obtained as 21.5 mS/mm at V_{GS} of −3 V. The on-state resistance (R_{ON}) was estimated as 147 Ω·mm.

The same MOSFET was separately measured at V_{GS} = 7 to −7 V and V_{DS} = 0 to −40 V (not shown here), and the maximum I_D was obtained as 270 mA/mm with an R_{ON} of 138 Ω·mm (obtained from the linear region of I_D at V_{GS} = −7 V), which is a reasonable value for a diamond MOSFET with an L_G of 2 µm and L_{SD} of 14.5 µm.

Fig. 2(b) shows the I_D-V_{GS} characteristics on a logarithmic scale. The on/off ratio was 10^6. The gate leakage current (I_G) was considerably low, $\leq 10^{-5}$ mA/mm. From the linear extrapolation of the $\sqrt{|I_D|}$–V_{GS} characteristics measured at a V_{DS} of −10 V, the normally-on operation was confirmed as the threshold voltage determined as 2.31 V. The subthreshold swing (SS) was determined to be 238 mV/dec, resulting in an interfacial density of states (D_{it}) of 6.4 × 10^{12} $eV^{-1}cm^{-2}$. The dielectric constant of the oxide layer was 6.2 and the oxide capacitance (C_{OX}) was 343 nF/cm^2.

Fig. 2(c) shows the off-state I_D and I_G characteristics of the MOSFET measured at a V_{GS} of 7 V. The high-voltage measurement was performed by submerging the MOSFET in a Fluorinert (FC-40) medium to avoid air arcing. The off-state I_D and I_G values were considerably low, and a breakdown voltage (V_{BR}) was measured to be 1406 V.

Figs 3(a) and (b) show the turn-on (t_{on}) and turn-off (t_{off}) dynamic switching characteristics presenting the input V_{GS}, output V_{DS} and I_D. A pulse generator supplied V_{GS} square-wave voltage varying from −3 V (on-state) to 3 V (off-state) at 100 Hz with a duty of 1%. A DC bias (V_{DD}) was 10.75 V and the load resistance, R_L, was 100 Ω. The DC bias was applied using the dry batteries. No external gate resistor was used. The

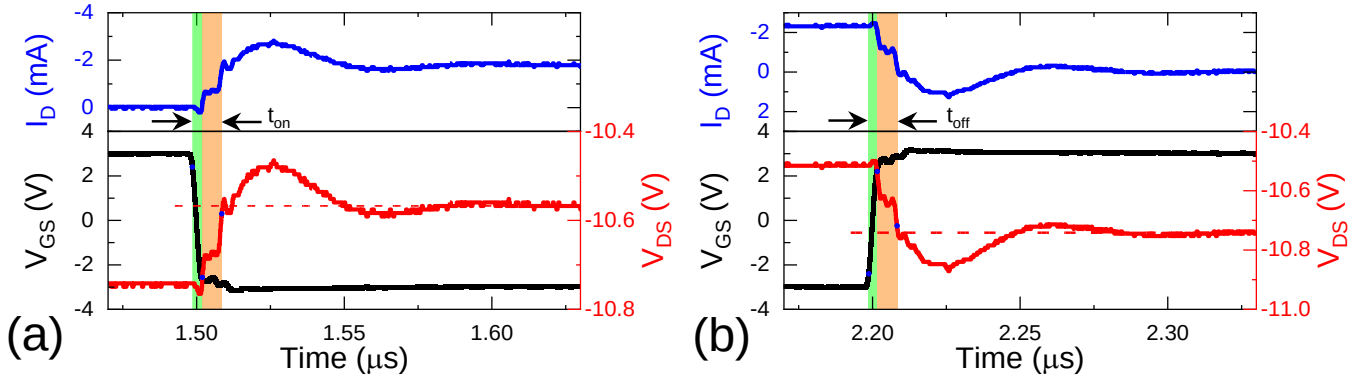

Fig. 3. (a)Turn-on, and (b) turn-off switching characteristics of the diamond MOSFET presenting V_{GS}, V_{DS}, and I_D.

internal gate resistance, R_G, was 10.98 Ω, and the gate-to-source resistance, R_{GS}, was ~23 GΩ. The t_{on} and t_{off} values were obtained from the switching characteristics as 9.97 ns and 9.63 ns, respectively.

t_{on} and t_{off} can be defined as $t_{on}= t_{d,on}+t_r$ and $t_{off}= t_{d,off}+ t_f$. The turn-on time delay ($t_{d,on}$) was determined as the time between 10% of V_{GS} (= 2.4 V) and 90% of V_{DS} (peak-to-peak). The time-rise (t_r) was the time taken to fall V_{DS} from 90% to 10%. Similarly, the turn-off time delay ($t_{d,off}$) was determined as the time from 90% of V_{GS} (= −2.4 V) to 10% of V_{DS} (peak to peak). The time-fall (t_f) was the time taken to rise the V_{DS} from 10% to 90%. The $t_{d,on}$ and $t_{d,off}$ values were determined as 3.37 ns and 2.93 ns, respectively and shaded in green color in Fig. 3. Time-rise (t_r) during turn-on and time-fall (t_f) during turn-off were respectively 6.60 ns and 6.70 ns and shaded in orange color in Fig. 3. Further, the energy loss during turn-on ($E_{on} = \int_{t_{on}} V_{DS}I_D dt$) was determined as 55.12 pJ and that at turn-off ($E_{off} = \int_{t_{off}} V_{DS}I_D dt$) was obtained as 153.18 pJ. Consequently, the total energy loss ($E_{on} + E_{off}$) becomes 208.30 pJ.

Furthermore, for R_L= 100 Ω, the load line was steep with respect to the measured drain current output (I_D-V_{DS}) characteristics. Consequently, in Fig. 3, I_D turns on/off within a small variation in V_{DS}. However, this V_{DS} variation and switching times increased with an increase in R_L. Fig. 4 shows the t_{on} and t_{off} values as a function of the R_L. The R_L was varied from 100 Ω to 10 kΩ. It seems that t_{on} and t_{off} both linearly increase with R_L; consequently, the power dissipation also increases. Possibly, owing to high R_{ON} of the MOSFET, switching times are almost proportional to R_L.

Interelectrode capacitances were measured at a frequency of 100 kHz, V_{GS} of 0 V, and V_{DS} of 10.75 V using Keysight 1505A. The gate-to-source (C_{GS}), drain-to-source (C_{DS}) and gate-to-drain (C_{GD}) capacitances were measured as 245 nF/mm, 715 pF/mm, and 17 pF/mm, respectively. The input capacitance, C_{iss} (= C_{GS} + C_{GD}), was determined as 245 nF/mm. The output capacitance, C_{oss} (= C_{DS} + C_{GD}), was obtained as 732 pF/mm. The reverse capacitance, C_{rss} (=C_{GD}), was 17 pF/mm.

It is well-known in other semiconductors that parasitic capacitances increase the switching times of MOSFET and subsequent switching power losses. The delay time can be explained as the charge and discharge times of C_{iss}. C_{oss} accounts for an additional energy loss due to its discharge in every switching cycle, and is estimated to be 1.9 nJ in this study. The C_{rss} is the so-called Miller capacitance that limits the rise and fall time. The fast-switching operation of the MOSFET was achieved by reducing the C_{rss} in SiC [27]. Fast-switching characteristics (<10 ns) of the diamond MOSFET were observed, probably owing to the low C_{rss} value. The C_{rss} was considerably low in this study due to the low dielectric constant (5.7) of diamond.

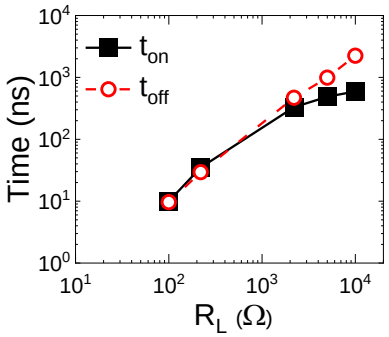

Fig. 4. Turn-on and turn-off time of the diamond MOSFET as a function of load resistance R_L.

Although the diamond MOSFET exhibited encouraging switching times, the development of device modules or packaging may be required for dynamic testing at high voltages of hundreds of volts in real applications.

IV. Conclusions

This study showed the dynamic switching characteristics of an NO_2 p-type doped diamond MOSFETs for the first time with a considerably short switching times t_{on} and t_{off} of respectively 9.97 and 9.63 ns indicating possible applications of diamond MOSFET in high-speed switching devices. The total energy loss owing to switching was estimated to be 208 pJ. The parasitic capacitances were measured as C_{iss}= 245 nF/mm, C_{oss}= 732 pF/mm, and C_{rss}=17 pF/mm. The MOSFET exhibited an I_D of 61 mA/mm at V_{GS} = − 3 V and V_{DS}= − 10 V, with a R_{ON} of 147 Ω·mm. The transfer characteristics showed a negligible gate leakage current, with an SS of 238 mV/dec.

References

[1] M. W. Geis, "Growth of device-quality homoepitaxial diamond thin films," *MRS Proc*, vol. 162, pp. 15–22, 1989, DOI: 10.1557/PROC-162-15.

[2] C. J. Wort and R. S. Balmer, "Diamond as an electronic material," *Mater. Today*, vol. 11, no. 1–2, pp. 22–28, Jan. 2008, DOI: 10.1016/S1369-7021(07)70349-8.

[3] Y. Yamamoto, T. Imai, K. Tanabe, T. Tsuno, Y. Kumazawa, and N. Fujimori, "The measurement of thermal properties of diamond," *Diam. Relat. Mater.*, vol. 6, no. 8, pp. 1057–1061, May 1997, DOI: 10.1016/S0925-9635(96)00772-8.

[4] J. Isberg, J. Hammersberg, E. Johansson, T. Wikström, D. J. Twitchen, A. J. Whitehead, S. E. Coe, and G. A. Scarsbrook, "High carrier mobility in single-crystal plasma-deposited diamond," *Science*, vol. 297, no. 5587, pp. 1670–1672, Sep. 2002, DOI: 10.1126/science.1074374.

[5] M. Kasu, K. Ueda, H. Ye, Y. Yamauchi, S. Sasaki, and T. Makimoto, "2 W/mm output power density at 1 GHz for diamond FETs," *Electron. Lett.* vol. 41, no. 22, p. 1249, Oct. 2005, DOI: 10.1049/el:20053194.

[6] S. Imanishi, K. Horikawa, N. Oi, S. Okubo, T. Kageura, A. Hiraiwa, and H. Kawarada, "3.8 W/mm RF power density for ALD Al_2O_3-based two-dimensional hole gas diamond MOSFET operating at saturation velocity," *IEEE Electron Device Lett.*, vol. 40, no. 2, pp. 279–282, Dec. 2019, DOI: 10.1109/led.2018.2886596.

[7] C. Yu, C. Zhou, J. Guo, Z. He, M. Ma, H. Yu, X. Song, A. Bu, and Z. Feng, "Hydrogen-terminated diamond MOSFETs on (001) single crystal diamond with state of the art high RF power density," *Functional Diamond*, vol. 2, no. 1, pp. 64–70, 2022, DOI: https://doi.org/10.1080/26941112.2022.2082853.

[8] X. Yu, J. Zhou, C. Qi, Z. Cao, Y. Kong, and T. Chen, "A high frequency hydrogen-terminated diamond MISFET with f_T/f_{MAX} of 70/80 GHz," *IEEE Electron Dev. Lett.*, vol. 39, no. 9, pp. 1373–1376, Aug. 2018, DOI: 10.1109/LED.2018.2862158.

[9] K. Ueda, M. Kasu, Y. Yamauchi, T. Makimoto, M. Schwitters, D. Twitchen, G. Scarsbrook, and S. Coe, "Diamond FET using high-quality polycrystalline diamond with f_T of 45 GHz and f_{max} of 120 GHz," *IEEE Electron Dev. Lett.*, vol. 27, no. 7, pp. 570–572, Aug. 2006, DOI: 10.1109/LED.2006.876325.

[10] M. Kubovic, M. Kasu, H. Kageshima, and F. Maeda, "Electronic and surface properties of H-terminated diamond surface affected by NO_2 gas," *Diam. Relat. Mater.*, no. 7, pp. 889–893, Sep. 2010, DOI: doi.org/10.1016/j.diamond.2010.02.021.

[11] T. Wade, M. W. Geis, T. H. Fedynyshyn, S. A. Vitale, J. O. Varghese, D. M. Lennon, T. Grotjohn, R. J. Nemanich, and M. A. Hollis, "Effect of surface roughness and H–termination chemistry on diamond's semiconducting surface conductance," *Diam. Rel. Mater.*, vol. 76, pp. 79–85, Jun. 2017, DOI: 10.1016/j.diamond.2017.04.012.

[12] M. Kasu, H. Sato, and K. Hirama, "Thermal stabilization of hole channel on H-terminated diamond surface by using atomic-layer-deposited Al_2O_3 overlayer and its electric properties," *Appl. Phys. Express*, vol. 5, no. 2, p. 025701, Feb. 2012, DOI: 10.1143/apex.5.025701.

[13] K. Hirama, H. Sato, Y. Harada, H. Yamamoto, and M. Kasu, "Diamond field-effect transistors with 1.3 A/mm drain current density by Al_2O_3 passivation layer," *Jpn. J. Appl. Phys.*, vol. 51, no. 9R, pp. 090112, Aug. 2012, DOI: 10.7567/jjap.51.090112.

[14] K. Hirama, H. Sato, Y. Harada, H. Yamamoto, and M. Kasu, "Thermally stable operation of H-terminated diamond FETs by NO_2 adsorption and Al_2O_3 passivation," *IEEE Electron Device Letters*, vol. 33, no. 8, pp. 1111–1113, Aug. 2012, DOI: 10.1109/LED.2012.2200230.

[15] N. C. Saha, S.-W. Kim, T. Oishi, and M. Kasu, "875-MW/cm² Low-Resistance NO_2 p-Type Doped Chemical Mechanical Planarized Diamond MOSFETs," *IEEE Electron Dev. Lett.*, vol. 43, no. 5, pp. 777–780, May 2022, DOI: 10.1109/LED.2022.3164603.

[16] N. C. Saha, S.-W. Kim, T. Oishi, Y. Kawamata, K. Koyama, and M. Kasu, "345-MW/cm^2 2608-V NO_2 p-type doped diamond MOSFETs with an Al_2O_3 passivation overlayer on heteroepitaxial diamond," *IEEE Electron Dev. Lett.*, vol. 42, no. 6, pp. 903–906, Apr. 2021, DOI: 10.1109/LED.2021.3075687.

[17] N. C. Saha, S.-W. Kim, T. Oishi, and M. Kasu, "3326-V modulation-doped diamond MOSFETs," *IEEE Electron Device Letters*, vol. 43, no. 8, pp. 1303–1306, Jun. 2022, DOI: 10.1109/LED.2022.3181444.

[18] N. C. Saha, S.-W. Kim, K. Koyama, T. Oishi, and M. Kasu, "3659-V NO_2 P-type doped diamond MOSFETs on misoriented heteroepitaxial diamond substrates," *IEEE Electron Device Letters*, pp. 1–1, Dec. 2022, DOI: 10.1109/LED.2022.3226426.

[19] M. Kasu, K. Ueda, H. Kageshima, and Y. Yamauchi, "RF equivalent-circuit analysis of P-type diamond field-effect transistors with hydrogen surface termination," *IEICE Transactions on Electronics*, vol. E91-C, no. 7, pp. 1042–1049, Jul. 2008, DOI: https://doi.org/10.1093/ietele/e91-c.7.1042.

[20] H. Kawarada, T. Yamada, D. Xu, H. Tsuboi, T. Saito, and A. Hiraiwa, "Wide temperature (10K–700K) and High Voltage (∼1000V) operation of C-H diamond MOSFETs for power electronics application," *2014 IEEE International Electron Devices Meeting*, Dec. 2014, DOI: 10.1109/IEDM.2014.7047030.

[21] M. Kasu, "Diamond Field-Effect Transistors for RF Power Electronics: Novel NO_2 hole doping and low-temperature deposited Al_2O_3 Passivation," *Japanese Journal of Applied Physics*, vol. 56, no. 1S, Dec 2016, DOI: 10.7567/JJAP.56.01AA01.

[22] M. W. Geis, T. C. Wade, C. H. Wuorio, T. H. Fedynyshyn, B. Duncan, M. E. Plaut, J. O. Varghese, S. M. Warnock, S. A. Vitale, and M. A. Hollis, "Progress toward diamond power field-effect transistors," *Physica Status Solidi (a)*, vol. 215, no. 22, p. 1800681, Nov. 2018, DOI: https://doi.org/10.1002/pssa.201800681.

[23] M. W. Geis, J. O. Varghese, M. A. Hollis, Y. Yichen, R. J. Nemanich, C. H. Wuorio, X. Zhang, G. W. Turner, S. M. Warnock, S. A. Vitale, R. J. Molnar, T. Osadchy, and B. Zhang, "Stable, low-resistance, 1.5 to 3.5 kω SQ−1, diamond surface conduction with a mixed metal-oxide protective film," *Diamond and Related Materials*, vol. 106, p. 107819, Jun. 2020, DOI: https://doi.org/10.1016/j.diamond.2020.107819.

[24] Y. Sasama, T. Kageura, M. Imura, K. Watanabe, T. Taniguchi, T. Uchihashi, and Y. Takahide, "High-mobility p-channel wide-bandgap transistors based on hydrogen-terminated diamond/hexagonal boron nitride heterostructures," *Nature Electronics*, vol. 5, no. 1, pp. 37–44, Dec. 2021, DOI: https://doi.org/10.1038/s41928-021-00689-4.

[25] S.-W. Kim, R. Takaya, S. Hirano, and M. Kasu, "Two-inch high-quality (001) diamond heteroepitaxial growth on sapphire ($11\bar{2}0$) misoriented substrate by step-flow mode," *Appl. Phys. Express*, vol. 14, no. 11, p. 115501, Oct. 2021, DOI: 10.35848/1882-0786/ac28e7.

[26] N. C. Saha and M. Kasu, "Improvement of the Al_2O_3/NO_2/H-diamond MOSFET by using Au gate metal and its analysis," *Diam. Relat. Mater.*, vol. 92, pp. 81–85, Feb. 2019, DOI: 10.1016/j.diamond.2018.12.017.

[27] Y. Saitoh, T. Masuda, H. Tamaso, H. Notsu, H. Michikoshi, K. Hiratsuka, S. Harada, and Y. Mikamura, "Switching performance of V-groove trench gate sic mosfets with grounded buried p+ regions," *Materials Science Forum*, vol. 897, pp. 505–508, May 2017, DOI: https://doi.org/10.4028/www.scientific.net/MSF.897.505.